THE JOURNAL OF PHYSICAL CHEMISTRY A

 VOLUME 106, NUMBER 39, OCTOBER 3, 2002

ARTICLES

Substituent Effects in Molecular Electronic Relaxation Dynamics via Time-Resolved Photoelectron Spectroscopy: $\pi\pi^*$ States in Benzenes

Shih-Huang Lee,[†,‡] Kuo-Chun Tang,[†] I-Chia Chen,[*,†] M. Schmitt,[§] J. P. Shaffer,[§] T. Schultz,[§] Jonathan G. Underwood,[§] M. Z. Zgierski,[§] and Albert Stolow[*,§]

Department of Chemistry, National Tsing Hua University, Hsinchu, Taiwan, ROC 30043, Institute of Atomic and Molecular Sciences, Academia Sinica, Taipei, Taiwan, ROC 10764, and Steacie Institute for Molecular Sciences, National Research Council of Canada, 100 Sussex Drive, Ottawa, ON, Canada K1A 0R6

Received: May 1, 2002

We study the applicability of femtosecond time-resolved photoelectron spectroscopy to the study of substituent effects in molecular electronic relaxation dynamics using a series of monosubstituted benzenes as model compounds. Three basic types of electronic substituents were used: C═C (styrene), C═O (benzaldehyde), and C≡C (phenylacetylene). In addition, the effects of the rigidity and vibrational density of states of the substituent were investigated via both methyl (α-methylstyrene, acetophenone) and alkyl ring (indene) substitution. Femtosecond excitation to the second $\pi\pi^*$ state leads, upon time-delayed ionization, to two distinct photoelectron bands having different decay constants. Variation of the ionization laser frequency had no effect on the photoelectron band shapes or lifetimes, indicating that autoionization from super-excited states played no discernible role. From assignment of the energy-resolved photoelectron spectra, a fast decaying component was attributed to electronic relaxation of the second $\pi\pi^*$ state, a slower decaying component to the first $\pi\pi^*$ state. Very fast electronic relaxation constants ($<$100 fs) for the second $\pi\pi^*$ states were observed for all molecules studied and are explained by relaxation to the first $\pi\pi^*$ via a conical intersection near the planar minimum. Although a "floppy" methyl substitution (α-methylstyrene, acetophenone) leads as expected to even faster second $\pi\pi^*$ decay rates, a rigid ring substitution (indene) has no discernible effect. The much slower electronic relaxation constants of the first $\pi\pi^*$ states for styrene and phenylacetylene are very similar to those of benzene in its first $\pi\pi^*$ state, at the same amount of vibrational energy. By contrast, the lifetime of the first $\pi\pi^*$ state of indene was much longer, attributed to its rigid structure. The second $\pi\pi^*$ state of benzaldehyde has a short lifetime, similar to the other derivatives. However, the relaxation of its first $\pi\pi^*$ state is orders of magnitude faster than that of the non-carbonyl compounds, due to the well-known presence of a lower lying nπ^* state. Methylation (acetophenone) leads to still faster first $\pi\pi^*$ state relaxation rates. These results fit very well with the current understanding of aromatic photophysics, demonstrating that time-resolved photoelectron spectroscopy provides for a facile, accurate and direct means of studying electronic relaxation dynamics in a wide range of molecular systems.

I. Introduction

The burgeoning area of *active* molecular scale electronics (MSE) involves the use of molecules or molecular assemblies acting as switches, transistors, or modulators.[1] A central theme is that structural rearrangement processes such as isomerization should lead to changes in either optical or electrical properties, generating the desired effect. These structural rearrangements are often proposed to be induced via electronic excitation. The

* To whom correspondence should be addressed. E-mail: albert.stolow@nrc.ca; icchen@mx.nthu.edu.tw.
† National Tsing Hua University.
‡ Academia Sinica.
§ National Research Council of Canada.

10.1021/jp021096h CCC: $22.00
Published on Web 09/11/2002

rational design of active MSE devices must include a detailed consideration of the dynamics of the "switching" process for several reasons. Foremost is that activation of the device (e.g. by a photon) must indeed lead to the desired change in optical or electrical properties, and therefore, this basic mechanism must be present. Two other issues, however, are of great practical significance. The *efficiency* of the molecular electronic process is a critical element because excited organic molecules often have a variety of complex decay paths that compete with the desired process. The efficiency of a device can be defined simply as the rate of the desired process divided by the sum of the rates of all competing processes. As certain of these competing processes can occur on ultrafast time scales (e.g., dissipation, dissociation), the rate of the desired process must be very fast indeed, even if the required overall response is slow. A directly related issue is that of *stability*. A molecular modulator that operates at 100 MHz and lasts for 3 years must switch $\sim 10^{16}$ times without "breaking". The quantum yields of any "harmful" processes must therefore be exceedingly small. Unfortunately, excited organic molecules have a number of destructive decay pathways, such as photodissociation and triplet formation (often leading to reaction). The relative rates and quantum yields of these processes, as well as their dependence on substituent and environmental effects, will be critical elements in the design of efficient, stable, *active* MSE devices. Techniques that allow for the direct determination of electronic relaxation rates will be useful in this regard.

Ultrafast electronic relaxation processes[2] play a central role in photochemistry and photobiology, internal conversion (IC) and intersystem crossing (ISC) being the two major nonradiative pathways. The tacit dynamical principle is the nonadiabatic coupling of electronic and vibrational motions. Due to the complexity of the interactions and the difficulties of spectroscopy in "real devices", it is often of interest to develop methods to study the details of excited-state electronic relaxation dynamics in isolated chromophores and model systems. The dependence of the nonadiabatic dynamics on substituent effects constitutes an important ingredient in understanding and predicting active MSE processes. In this paper, we present an experimental study of substituent effects on electronic relaxation dynamics in a series of model compounds using time-resolved photoelectron spectroscopy (TRPES). Our main purpose here is to demonstrate that this experimental method allows for *facile*, *accurate*, and *direct* determination of electronic relaxation rates in polyatomic molecules and to verify that our results fit very well with the current understanding of these dynamics. Secondarily, we hope that these types of phenomenological studies can contribute toward the development of "basic rules" governing substituent effects in active MSE processes.

Femtosecond TRPES (for a recent review, see ref 3) appears to be emerging as a powerful technique for the study of electronic relaxation dynamics in isolated molecules, as it allows for the study of sequential ultrafast electronic processes in *both* optically bright and dark states. Its application to polyatomic nonadiabatic dynamics was proposed theoretically over 10 years ago[4] and first demonstrated for the case of S_1-S_0 internal conversion in hexatriene.[5] TRPES has been applied to wave packet dynamics in simple systems,[6−10] intramolecular vibrational energy redistribution,[11] internal conversion,[12−18] photodissociation dynamics,[19,20] intersystem crossing,[21,22] intracluster reaction dynamics,[23] and excited-state intramolecular proton-transfer dynamics.[24] The outgoing photoelectron may also be differentially analyzed as a function of time with respect to angular distribution.[22,25−27] Additionally, time-resolved photoelectron-photoion coincidence (PEPICO)[16] and photoelectron−photoion coincidence-imaging[28] spectroscopies have been demonstrated.

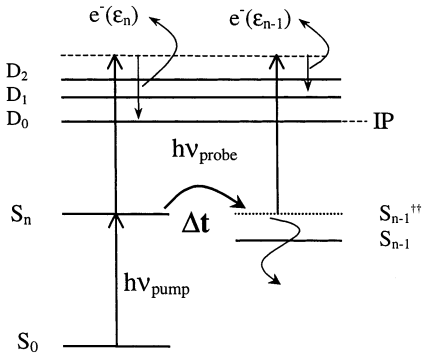

Figure 1. An electronic energy level diagram and the femtosecond pump−probe time-resolved photoelectron spectroscopy scheme. S_n and S_{n-1} are nonadiabatically coupled singlet states; $n = 2$ or 3, depending on the molecule. D_0, D_1, and D_2 represent the ground and two lowest cation electronic states. S_{n-1}* denotes the vibrationally excited S_{n-1} state formed by the electronic relaxation process. S_{n-1}* itself electronically relaxes to lower lying states via subsequent nonadiabatic processes. S_n and S_{n-1} can, depending on the Koopmans' correlations, ionize into different cationic states. Time-resolved photoelectron spectroscopy allows for *direct* measurement of these sequential electronic relaxation processes. For a discussion, see the text.

Photoelectron spectroscopy is sensitive to both electronic configurations and vibrational dynamics.[29] The well-known Koopmans' picture is based upon the approximation that photoionization is a single-photon, single active electron process and that the remaining electrons (which form the ion "core") are unchanged during this process.[29] The Koopmans' picture suggests that specific electronic configurations of the neutral molecule correlate, upon ionization, with specific cation electronic states. In excited-state nonadiabatic dynamics, there is a change in zeroth-order electronic configuration upon internal conversion (IC) or intersystem crossing (ISC), accompanied by a large change in vibrational energy. Making use of Koopmans'-type correlations, femtosecond TRPES has been demonstrated to disentangle vibrational dynamics from the coupled electronic (population) dynamics in ultrafast nonadiabatic processes, allowing for a *direct* view of electronic relaxation processes.[13,14,30]

In Figure 1, we show a generic energy level diagram and the TRPES scheme. An excited-state S_n is prepared by a femtosecond pump laser. The S_n state is nonadiabatically coupled to a lower lying state S_{n-1}, leading to an electronic relaxation process. The two coupled electronic states are photoionized after a time delay Δt by a femtosecond probe laser and the photoelectron spectrum, containing bands $e^-(\epsilon_n)$ and $e^-(\epsilon_{n-1})$, is measured. Two limiting cases have been identified: type I, the favorable case of complementary ionization correlations,[17] and type II, the unfavorable case of corresponding ionization correlations.[18] In type I systems, the two nonadiabatically coupled electronic states S_n and S_{n-1} correlate upon ionization to *different* cation electronic states (e.g., $S_n \rightarrow D_0$, $S_{n-1} \rightarrow D_1$). As long as the two cation states are energetically well separated, this situation favors the disentangling of electronic from vibrational dynamics. The electronic relaxation dynamics in S_n and S_{n-1} may be clearly and separately determined. For a more detailed discussion, see ref 17. In type II systems, the two nonadiabatically coupled electronic states S_n and S_{n-1} correlate upon ionization to the *same* cation electronic states (e.g., $S_n \rightarrow D_0$, $S_{n-1} \rightarrow D_0$). In this case, the ability to extract the electronic relaxation dynamics in each state depends strongly on the

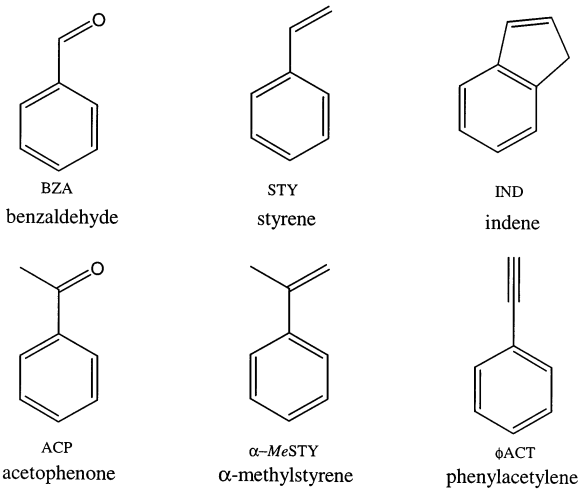

Figure 2. Molecular structures of the monosubstituted benzenes used in this work. Three different electronic substituents were used, C═O, C═C, and C≡C, leading to different state interactions. The effects of vibrational dynamics were investigated via the use of methyl group (floppier), as in α-MeSTY and ACP, or a ring structure (more rigid), as in IND, side group additions. As shown in Table 2, BZA and ACP have favorable type I ionization correlations, whereas STY, IND, α-MeSTY (same as STY), and ϕACT have unfavorable type II ionization correlations.

Franck−Condon displacements (geometry changes) upon nonadiabatic crossing and ionization. Of relevance to this paper, if the molecular frame is fairly rigid and the displacements are small, then there will be a tendency to conserve the vibrational quantum number upon ionization. Since the nonadiabatic process converts the electronic energy of S_n into vibrational energy within S_{n-1}, the excess vibrational energy will appear as a downshift in the photoelectron spectrum, allowing at least partial deconvolution of the electronic relaxation dynamics in each state. For a more detailed discussion, see ref 18.

In the following, we present a TRPES study of electronic relaxation dynamics in a series of monosubstituted benzenes. We concern ourselves in the present study only with *electronic* population dynamics and integrate over any vibrational dynamics within each electronic state. To emphasize the effects of substituents on ultrafast electronic relaxation dynamics, we focus on the first and second $\pi\pi^*$ states of these aromatic systems and on substituents that are expected to have electronic effects. We chose six benzene derivatives, shown in Figure 2—benzaldehyde (BZA), styrene (STY), indene (IND), acetophenone (ACP), α-methylstyrene (α-MeSTY), and phenylacetylene (ϕACT). This choice of substituents allowed us to address two main points: (1) the effect of the substituent on the electronic states and couplings and (2) the effect of the substituent on the rigidity or floppiness of the molecular frame. Three electronically distinct substituents were chosen: C═O, C═C, and C≡C. For the C═C, potential off-axis conjugation effects with the ring in STY can be contrasted with the lack of these in the C≡C of ϕACT. For the heteroatomic substituent C═O, the influence of the additional $n\pi^*$ state on the $\pi\pi^*$ dynamics is investigated by comparing BZA with STY and ACP with α-MeSTY. The effects of vibrational dynamics and densities-of-states on the electronic relaxation rates were studied via both methyl ("floppier") and alkyl ring ("more rigid") substitution: STY is compared with both the floppier α-MeSTY and the much more rigid IND; BZA is compared with the floppier ACP. We compare the results of our *direct* measurements with existing values for benzene and place them in the context of the accepted understanding of aromatic photophysics in order to validate our general experimental approach.

II. Photophysics of Benzenes

The understanding of nonadiabatic dynamics in aromatics is quite well developed. There have been many experimental and theoretical studies of S_1 electronic relaxation—both S_1-S_0 IC and S_1-T_1 ISC—in gaseous aromatic molecules. For molecules such as benzene, naphthalene, anthracene, tetracene, and their derivatives,[31] S_1-T_1 ISC is the predominant electronic relaxation channel at small excitation energies where it is favored by Franck−Condon (FC) factors. Benzene, for example, has a long lifetime of 106 ns at its S_1 origin.[32] The effect of ring heteroatoms can be seen in the azabenzenes pyridine, pyrazine, and pyrimidine, which have much shorter lifetimes, 42 ps, 119 ps, and 1.8 ns respectively,[33] at their S_1 origin, due to the presence of low-lying $n\pi^*$ states. That azabenzenes have a higher phosphorescence quantum yields and relatively lower fluorescence quantum yields at their S_1 origin is likewise explained by the strong spin−orbit coupling between the $n\pi^*$ and $\pi\pi^*$ states, leading to enhanced ISC rates.[34−36]

Increased vibrational energy leads to both quantitative and qualitative changes in electronic relaxation dynamics. In benzene,[37−40] a rapidly increasing electronic relaxation rate at larger excitation energy, the so-called "channel-three" decay, is attributed to S_1-S_0 IC.[41,42] The threshold for channel-three decay in benzene is approximately 3000 cm^{-1} above the $S_1(\pi\pi^*)$ origin. With increasing size, the channel-three threshold falls in the order benzene < naphthalene < anthracene < tetracene. Sobolewski et al.[43] performed quantum-chemical calculations on potential energy surfaces (PES) for benzene isomerization to prefulvene (diradical form); they concluded that the S_1 PES minimum is separated from that of prefulvene by a 3750 cm^{-1} barrier, in accordance with the threshold for channel-three decay in benzene. The proposed IC pathway starts at the S_1 minimum geometry and then overcomes—tunnels through—the transition state to prefulvene, whereupon it enters the S_0 surface via S_1-S_0 IC. Strong repulsion between S_1 and S_0 surfaces along the coupling coordinate contributes to the lack of a potential barrier from prefulvene to S_0 benzene.

There exist few direct measurements of the lifetimes of the second $\pi\pi^*$ states in benzene derivatives. The $S_2(\pi\pi^*)$ electronic relaxation of several aromatic molecules—benzene,[12] benzene dimer,[44] benzene(ammonia)$_n$ clusters,[45] phenol,[15] azobenzene,[46] naphthalene[18] and phenanthrene[18]—has been recently investigated. [N.B., in nonaromatic systems, studies have been carried out on S_2 electronic relaxation dynamics in polyenes[47] such as butadiene, [48] *Z*(*E*)-hexatriene,[5,49] *EZ*(*ZE*)-octatriene,[50] octatetraene,[51,52] decatetraene,[14,17,30,53,54] and longer polyenes.[55−57]] These aromats typically show a subpicosecond lifetime for the $S_2(\pi\pi^*)$ state with a much longer lifetime for the $S_1(\pi\pi^*)$ state. In general, the S_2 states might be expected to exhibit greater sensitivity to the electronic structure of the substituent than do the S_1 states, which decay predominantly as does benzene. Previously reported experimental values of the first and second $\pi\pi^*$ state electronic energies[58−62] and the ionization potentials (IP)[63−67] for the molecules studied here are given in Table 3.

A simplified picture of the four lowest $\pi\pi^*$ transitions in benzene, based on one-electron molecular orbitals, is obtained from the Platt perimeter model.[68] The inclusion of configuration interaction in quantum-chemical calculations of benzene in these four states, degenerate in zeroth order, yields states with energy order $L_b(S_1, B_{2u}) < L_a(S_2, B_{1u}) < B_a, B_b(E_{1u})$.[61] Transitions to states B_a and B_b are electric dipole-allowed, but those to states

TABLE 1: Calculated Excited State Energies and State Symmetries of Some Monosubstituted Benzenes[a]

	1	2	3	4	5	6	7	8	9	10
BZA	T_1 (1A″) 3.14	T_2 (1A′) 3.30	**S_1 (1A″) 3.69**	T_3 (2A′) 4.00	T_4 (3A′) 4.46	**S_2 (2A′) 4.78**	T_5 (4A′) 5.15	**S_3 (3A′) 5.31**	S_4 (2A″) 5.68	S_5 (4A′) 6.41
ACP	T_1 (1A″) 3.21	T_2 (1A′) 3.36	**S_1 (1A″) 3.7**	T_3 (2A′) 4.07	T_4 (3A′) 4.46	**S_2 (2A′) 4.83**	T_5 (4A′) 5.13	S_3 (3A′) 5.32	S_4 (2A″) 5.62	S_5 (4A′) 6.38
STY	T_1 (1A′) 2.88	T_2 (2A′) 4.19	T_3 (3A′) 4.35	T_4 (4A′) 4.73	T_5 (5A′) 4.84	**S_1 (2A′) 4.93**	**S_2 (3A′) 5.14**	S_3 (4A′) 6.03	S_4 (5A′) 6.54	S_5 (6A′) 6.73
IND	T_1 (1A′) 2.97	T_2 (2A′) 4.15	T_3 (3A′) 4.30	T_4 (4A′) 4.66	**S_1 (2A′) 4.86**	T_5 (5A′) 4.87	**S_2 (3A′) 5.02**	S_3 (4A′) 5.87	S_4 (5A′) 6.43	S_5 (6A′) 6.55
ϕACT	T_1 (1A′) 3.24	T_2 (2A′) 4.41	T_3 (3A′) 4.43	T_4 (4A′) 4.83	T_5 (5A′) 4.97	**S_1 (2A′) 5.07**	**S_2 (3A′) 5.28**	S_3 (1A″) 5.36	S_4 (4A′) 6.29	S_5 (2A″) 6.35

[a] TD/B3LYP/6-31G* *vertical* excitation energies (in eV) at the B3LYP/6-31G*-optimized S_0 geometry. The electronic relaxation dynamics of states marked in bold were studied in this work.

TABLE 2: Calculated Cation State Energies and Symmetries of Some Monosubstituted Benzenes[a]

	0 (IP)	1	2	3	4	5	Koopmans' correlations	
BZA	D_0 (1A″) 9.22 eV	D_1 (1A′) +0.03 eV	D_2 (2A″) +0.11 eV	D_3 (2A′) +2.53 eV	D_4 (3A′) +2.56 eV	D_5 (4A′) +2.72 eV	S_2 , $S_3 \rightarrow D_0, D_2 + e^-$ $S_1 \rightarrow D_1, D_3 + e^-$	type I
ACP	D_0 (1A′) 8.85 eV	D_1 (1A″) +0.07 eV	D_2 (2A″) +0.23 eV	D_3 (2A′) +2.63 eV	D_4 (3A′) +2.76 eV	D_5 (3A″) +2.77 eV	$S_2 \rightarrow D_1, D_2 + e^-$ $S_1 \rightarrow D_0, D_3 + e^-$	type I
STY	D_0 (1A″) 7.88 eV	D_1 (2A″) +1.19 eV	D_2 (3A″) +2.48 eV	D_3 (1A′) +3.39 eV	D_4 (2A′) +3.74 eV	D_5 (4A″) +3.95 eV	$S_2 \rightarrow D_0, D_1 + e^-$ $S_1 \rightarrow D_0, D_1 + e^-$	type II
IND	D_0 (1A″) 7.59 eV	D_1 (2A″) +1.20 eV	D_2 (3A″) +2.53 eV	D_3 (1A′) +3.42 eV	D_4 (4A″) +3.87 eV	D_5 (2A′) +3.93 eV	$S_2 \rightarrow D_0, D_1 + e^-$ $S_1 \rightarrow D_0, D_1 + e^-$	type II
ϕACT	D0 (1A″) 8.21 eV	D1 (2A″) +0.63 eV	D2 (1A′) +1.31 eV	D3 (3A″) +2.42 eV	D4 (2A′) +3.22 eV	D5 (3A′) +3.46 eV	$S_2 \rightarrow D_0, D_1 + e^-$ $S_1 \rightarrow D_0, D_1 + e^-$	type II

[a] TD/B3LYP/6-31G* vertical excitation energies (eV) at the B3LYP/6-31G* optimized D_0 geometry. The cation excited state energies (D_{1-5}) are given relative to the *vertical* IP. The Koopmans' correlation indicates the channel expected for single photon, single active electron ionization. Only the electronic channels D_{0-2} were open in these experiments.

TABLE 3: Experimentally Determined Electronic Relaxation Time Constants (τ) and Energetics for Benzene and Its Monosubstituted Derivatives

		2nd $\pi\pi^*$	1st $\pi\pi^*$	2nd $\pi\pi^*$		1st $\pi\pi^*$	
	IP (eV)[a]	E (eV)[a]	E (eV)[a]	τ (fs)[b,c]	vib energy (cm^{-1})	τ (ps)[b,c]	vib energy (cm^{-1})
benzene	9.24	6.05	4.75	50	1210	6.7	11690
STY	8.46	4.88	4.31	**52(5)**	0	**88(8)**	4550
α-MeSTY	8.50	n/a	n/a	**18(3)**	0	**39(3)**	~4600
IND	8.14	4.76	4.31	**43(5)**	920	**274(9)**	4550
ϕACT	8.83	5.20	4.45	**54(7)**	0	**63(5)**	5800
						9.4(7)	9860
BZA	9.57	5.13	4.36	**67(6)**	0	**0.440(8)**	0
						0.340(7)	406
						0.300(7)	955
						0.125(8)	6140
ACP	9.38	5.17	4.39	**n/a**	n/a	**0.14(1)**	0

[a] Energetics and time constants for benzene are taken from ref 12. Energetics for styrene are from refs 58, 61, 63; α-methylstyrene, ref 64; indene, refs 62, 65; phenylacetylene, refs 58, 61, 63; benzaldehyde, refs 58, 59, 66; and acetophenone, refs 58, 60 and 67. [b] The uncertainty ($\pm 1\sigma$) is in units of the last significant figure. [c] Items in bold are from this work.

L_a and L_b are forbidden for one-photon transitions from the electronic ground electronic state S_0. L_a and L_b are vibronically allowed via e_g stretching and e_g bending modes, respectively. For the molecules studied here (C_s or C_{2v} symmetry), both L_a and L_b become symmetry-allowed for one-photon transitions from the ground state, but the energetic ordering of L_a and L_b depends on the nature of the substituents on the phenyl ring. Discrete vibrational bands were observed in the first $\pi\pi^*$ transitions for these molecules. For instance, according to a rotational analysis of the S_0–S_1 fluorescence excitation spectra of STY and ϕACT,[61] the $S_1(\pi\pi^*)$ origin band in ϕACT has a b-type structure, like that of most monosubstituted benzenes, whereas the corresponding band in STY has an a-type structure. Thus, the $S_1(\pi\pi^*)$ state of ϕACT has L_b character, but the $S_1(\pi\pi^*)$ state of STY has L_a character. This reversal of the electronic character in S_1 STY was attributed to the presence of off-axis conjugation with the C=C group.[61] The $S_0 \leftarrow S_1$ transition moment polarization in ϕACT is along the axis perpendicular to the ϕ-C≡CH bond (L_b). It changes to almost parallel (L_a) to the ϕ-C=*C* axis in STY, due to conjugation with the HC=CH_2 group. In STY, the S_1 and S_2 states have such similar transition moment polarizations that the differentiation into L_a and L_b essentially vanishes. In vapor-phase absorption spectra of IND,[62] the origin of the $S_1(\pi\pi^*)$ transition is in accord with that determined in a supersonic jet by resonance-enhanced multiphoton ionization.[65]

A recent study combined TRPES with coincident detection of ions and electrons to observe IC of the $S_2(\pi\pi^*)$ state in benzene,[12] benzene dimers,[44] and benzene(ammonia)$_n$ clusters.[45] It appeared that direct $S_2(\pi\pi^*)-S_0$ IC dominates over $S_2(\pi\pi^*)-S_1(\pi\pi^*)$ IC. The reported lifetimes of benzene were 50 fs and 6.7 ps for $S_2(\pi\pi^*)$ and $S_1(\pi\pi^*)$ states with vibrational energy 1210 and 11690 cm^{-1}, respectively. The S_2-S_1 and S_1-S_0 conical intersections of benzene[69] were calculated with an MC–

SCF method using a 4-31G basis set; the S_1-S_0 crossing surface extends into the vicinity of the S_2-S_1 conical intersection, which is near the $S_2(\pi\pi^*)$ minimum. In $S_2(\pi\pi^*)$ electronic relaxation, the subsequent S_1-S_0 decay occurs via passage through an efficient S_2-S_1 conical intersection. In the benzene dimer,[12] the $S_2(\pi\pi^*)$ lifetime of 40−50 fs is similar to that of the monomer, but the $S_1(\pi\pi^*)$ decay is prolonged to 100−300 ps. Likewise, for benzene(ammonia)$_n$ clusters,[45] the $S_2(\pi\pi^*)$ lifetime of 100 fs is slightly longer than that of benzene monomer, and the $S_1(\pi\pi^*)$ relaxation is also prolonged up to 100 ps as in the benzene dimer. Of interest to the present study, hindered out-of-plane motion in these clusters could potentially restrict vibrational motions, leading to the S_1-S_0 conical intersection funnels, thus increasing the S_1 lifetime.

III. Experimental Section

The experimental arrangement is described in detail elsewhere.[70] Briefly, in this work we employed a broadly tunable femtosecond laser system combined with a supersonic molecular beam magnetic bottle photoelectron TOF spectrometer in order to measure electronic relaxation dynamics in monosubstituted benzene derivatives.

The femtosecond laser system consists of a Ti:sapphire oscillator (Spectra Physics, Tsunami, 830 nm, 70fs) pumped by a diode-pumped Nd:YLF laser (SP, Millennia). The oscillator seeded a Ti:Sa regenerative amplifier (Positive Light, Spitfire) pumped by a 1 kHz Nd:YLF laser (Positive Light, Merlin). This output was further amplified in a two-pass linear Ti:Sa amplifier (Positive Light) pumped by a second Nd:YLF laser (Positive Light, Merlin) to yield 2.5 mJ, 830 nm compressed, 70 fs pulses at a 1 kHz rate. Broadly tunable radiation was obtained from two optical parametric amplifiers (Quantronix/Light Conversion, TOPAS). The femtosecond signal and idler outputs of these were externally sum-mixed with a separate 830 nm femtosecond pulse to generate visible light. After frequency doubling or sum-mixing with a separate 415 nm femtosecond pulse, both pump and probe UV beams were generated. A 208 nm probe pulse was generated directly by frequency quadrupling of a fundamental 830 nm pulse. In all cases both pump and probe UV beams were recompressed in a double-prism configuration before being collinearly combined with a dichroic beam splitter. Importantly, the UV intensities used in these experiments were kept below 1×10^{11} W/cm^2 in order to avoid multiphoton ionization and strong field (ponderomotive) effects on the photoelectron spectra.[71] This was achieved by using a long focal length ($f = 80$ cm) Al mirror to mildly focus the pump and probe pulses into the interaction region of the photoelectron spectrometer.

The molecular beam photoelectron spectrometer consists of a high-intensity molecular beam source chamber, a differentially pumped interaction region (with a 1 T electromagnet for 2π electron collection), and a differentially pumped solenoidal (1 mT field) electron time-of-flight tube with a microchannel plate detector. The source chamber (base pressure 2×10^{-7} Torr) was pumped by four Edwards EO250 Diffstak diffusion pumps (net speed = 10 000 L/s), and a continuous molecular beam was generated with a nozzle (diameter 0.5 mm) and a 0.3 mm diameter skimmer. A 1 mm skimmer located in the turbo-pumped (Seiko-Seiki STP400C) UHV interaction chamber (base pressure 2×10^{-9} Torr) helped to collimate the molecular beam through the magnet pole pieces. Photoelectrons emitted into the upper hemisphere were parallelized by the highly divergent 1 T magnetic field at the interaction point and then guided to the detector by the 10 G solenoidal guiding magnetic field along the turbo-pumped (Seiko-Seiki) UHV electron drift tube (base pressure 2×10^{-10} Torr). To minimize deleterious surface potential effects, in vacuo bake-out lamps in the UHV regions kept interior surfaces of the spectrometer hot (80−100 °C) at all times to maintain constant energy calibration over extended periods. Benzaldehyde, acetophenone, styrene, α-methylstyrene, indene, and phenylacetylene (all Aldrich) were used without further purification. During experiments, glass reservoirs of styrene, α-methyl styrene, and phenylacetylene were kept at 22 °C, benzaldehyde at 52 °C, acetophenone at 65 °C, and indene at 65 °C in order to obtain optimal seed ratios for the molecular beam expansion. The organic vapor was seeded in He at a stagnation pressure of typically 300−500 Torr.

Single photoelectrons were timed and counted using a 300 MHz discriminator with a 500 ps/bin resolution multichannel scaler (FastCOMTEC 7886). The TOF measurement permitted each laser shot to be rapidly transferred to a computer for active laser energy filtering, one-color background subtraction, and data normalization. Data were discarded if the corresponding energy of either the pump or probe laser pulse fluctuated by greater than 30% from the mean. The pump−probe photoelectron spectra, recorded as a function of time delay, were obtained by subtraction of one-color (i.e. pump alone and/or probe alone) background spectra at *each* time step and normalized with respect to fluctuations in laser pulse energy and molecular beam intensity. Photoelectron energies were calibrated via the well-known two-photon nonresonant photoelectron spectrum of NO. *trans*-1,3-Butadiene (C_4H_6) has a S_2 state lifetime of approximately 15 fs, estimated from a width of 980 cm^{-1} fwhm for the origin band.[48] As this is much shorter than the ∼100−150 fs UV laser pulses used in the present work; it was used to determine the pump−probe cross-correlation (instrument response) function and the absolute pump−probe time zero ($\Delta t = 0$). The nonresonant ionization of NO gave similar cross-correlation functions (CC). In these experiments, the CC had fwhm in the 130−210 fs range, depending on the nonlinear mixing scheme used. The CC were measured for *each* experiment and are plotted along with the time-resolved data for each molecule. In the data analysis, the electronic lifetime of butadiene $\tau_b = 15$ fs was taken into account in the temporal response of the CC. The origin bands of the second $\pi\pi^*$ electronic transitions were excited for all molecules, except for α-methylstyrene (near origin) and indene (920 cm^{-1} above the origin). Several different vibrational levels of the first $\pi\pi^*$ state were directly excited for the cases of benzaldehyde and acetophenone. To investigate the possibility that the extracted time constants were sensitive to the photoionization dynamics (i.e., direct vs possible autoionization of superexcited states), we varied the probe laser photon energy significantly. No sensitivity of the fits to the probe laser wavelength was observed in these cases.

IV. Results and Analysis

In Figure 1, S_n is the electronic term value of the nth singlet state and D_j is the electronic energy of the jth doublet state of the cation. Jet-cooled ground state (S_0) molecules were optically excited to electronic state S_n with a femtosecond pump pulse $h\nu_{pump}$, thus forming a wave packet. After a time delay Δt, the wave packet in the nonadiabatically coupled S_n/S_{n-1} manifolds was projected onto the ionization continuum with a single photon from a femtosecond probe pulse $h\nu_{probe}$. The emitted electrons ϵ_n and ϵ_{n-1} were then energy analyzed using the time-of-flight (TOF) technique. Only cation states D_j with $j \leq 2$ were energetically accessible in these experiments. The electronic

relaxation process transforms the electronic energy difference $\Delta E(S_n - S_{n-1})$ into vibrational energy within S_{n-1}, which itself subsequently decays via a secondary electronic relaxation process. Photoelectron spectroscopy completely (or partially, depending on the molecule) separates the two bands: ϵ_n corresponding to the higher E_{kin} region and ϵ_{n-1} to the lower E_{kin} region of the spectrum. We integrated over each photoelectron band ϵ_n and ϵ_{n-1} in order to extract the time dependence of the electronic populations of S_n and S_{n-1}, as we concern ourselves solely with the electronic population dynamics at present.

To discern the substituent effects on the electronic level structure, we have carried out quantum chemical calculations at the TD/B3LYP/6-31G* level on the neutral excited states of BZA, ACP, STY, IND, and ϕACT. We calculated the vertical excitation energies at the optimized B3LYP/6-31G* S_0 ground-state geometry for the first seven neutral electronic states (singlets and triplets) and for the next three lowest singlet states. These are given, along with their state symmetries, in Table 1. It can be seen that $S_2 \rightarrow S_1$ electronic relaxation in BZA and ACP will be promoted by antisymmetric modes, whereas in STY, IND, and ϕACT, it will be promoted by symmetric modes. Additionally, due to the proximity of low lying triplet states of A′ symmetry in BZA and ACP, it is expected that the S_1 (A″) singlet states of these molecules will undergo rapid intersystem crossing. By contrast, the lower lying triplet states in STY, IND, and ϕACT have the same symmetry (A′) as the S_1(A′) state. Therefore, the S_1 states of these molecules are expected to undergo slow (due to the large gap) internal conversion to the S_0 ground state, rather than ISC.

To discern the Koopmans' ionization correlations used in the TRPES assignments, we have also calculated the vertical ionization potentials at the optimized B3LYP/6-31G* S_0 ground-state geometry and cation vertical excited-state energies at the optimized B3LYP/6-31G* D_0 ground-state geometry for the first five doublet cation electronic states of BZA, ACP, STY, IND, and ϕACT. These are given, along with their state symmetries, in Table 2. We now consider Koopmans'-type electronic correlations in the photoionization dynamics, using BZA as an example. The S_2 state of BZA is a $\pi\pi^*$ state. Therefore, removal of the excited electron leaves a π-hole ion core (a π^{-1} configuration). By contrast, the S_1 state of BZA is a $n\pi^*$ state and removal of the excited electron leaves an n-hole ion core (an n^{-1} configuration). The D_0 cation state is a A″ π^{-1} configuration and the D_1 cation state is an A′ n^{-1} configuration. Therefore, the expected Koopmans' ionization correlations are $S_2 \rightarrow D_0$ and $S_1 \rightarrow D_1$, as indicated in the right-hand column of Table 2. The Koopmans' correlations for the other molecules were obtained via similar arguments. It can be seen that the S_2 and S_1 states in BZA and ACP have type I (complementary) correlations,[17] favoring the energetic separation of the two ionization channels and allowing for direct observation of the electronic population dynamics in each state, as was seen for the case of $S_2 \rightarrow S_1$ internal conversion in *all-trans*-decatetraene.[13,14,17]

The S_2 and S_1 states in STY, IND, and ϕACT, by contrast, exhibit type II (corresponding) ionization correlations.[18] The two states have a propensity to ionize into the same continua, making the direct observation of the electronic relaxation in each state more challenging. We note, however, that in these rather rigid aromatic molecules, the molecular and cationic orbitals under consideration are essentially all localized on the benzene ring. The geometries of the cations resemble those of corresponding neutral species, and the ionizing transitions thus tend to have limited vibrational progressions. In such cases, the two photoelectron bands will approximately reflect the vibrational energy content of the state being ionized. Due to the significant increase in vibrational energy upon internal conversion, this effect is often sufficient to allow separate monitoring of the electronic relaxation dynamics in the two states, as was seen for the case of $S_2 \rightarrow S_1$ internal conversion in phenanthrene.[18]

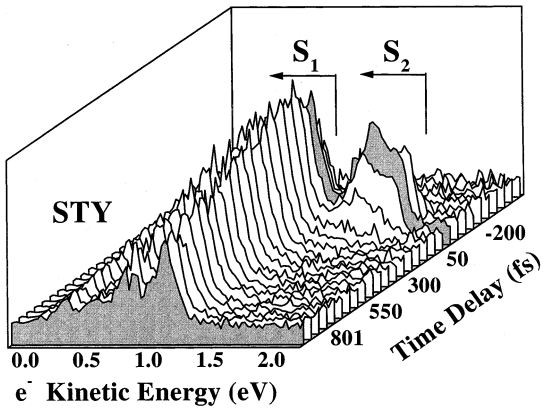

Figure 3. A typical time-resolved photoelectron spectrum, shown here for STY with $\lambda_{pump} = 254.3$ nm and $\lambda_{probe} = 218.5$ nm. The energetics and IP allow for assignment of the photoelectron bands to ionization of $S_2(\pi\pi^*)$ and $S_1(\pi\pi^*)$, as indicated. Due to the rigidity of the benzene ring, the change in vibrational energy upon internal conversion is immediately apparent as a downshift in electron kinetic energy, despite the fact that STY has unfavorable type II ionization correlations. The S_2 state can be seen to decay on ultrafast time scales. The S_1 state decays on a much longer (ps) time scale. For a discussion, see the text.

A typical example of a time-resolved photoelectron spectrum, STY at $\lambda_{pump} = 254.3$ nm and $\lambda_{probe} = 218.5$ nm, is shown in Figure 3. All time-resolved photoelectron spectra for all molecules studied here have similar signal-to-noise ratios. Using the reported electronic energies of first and second $\pi\pi^*$ states and ionization potential of STY (see Table 3), we were able to assign the photoelectron band in the higher $E_{kin} = 0.6-1.0$ eV energy range to $S_2(\pi\pi^*)$ ionization and that in the lower $E_{kin} \leq 0.6$ eV energy range to $S_1(\pi\pi^*)$ ionization. It can be seen that the $S_1(\pi\pi^*)$ component grows in rapidly, corresponding to the ultrafast internal conversion of the $S_2(\pi\pi^*)$ component. The $S_1(\pi\pi^*)$ component subsequently decays on a much longer picosecond time scale (not shown). It can be seen that despite STY being an unfavorable type II photoionization case, the two bands are well enough resolved to allow for unambiguous separation of the two channels and determination of the sequential electronic relaxation time scales.

In Figures 4−10, we show the time-dependence of the photoelectron bands ϵ_n and ϵ_{n-1}, obtained in the manner described above, for each of the molecules studied. In all figures we show the cross-correlation function (open circle data points) for that particular measurement. To study the effects of the initial vibrational energy, three different vibrational states of benzaldehyde (BZA) in its first (S_2) $\pi\pi^*$ state were excited: 0^0, 24^1, 20^1, shown in Figure 4a−d. It can be seen (discussed in detail below) that the electronic relaxation rate increases with increasing vibrational excitation. To demonstrate that these results are not dependent on the ionization dynamics, we show in Figure 4c a repeat of the S_2 0^0 excitation but for a different probe wavelength (i.e., 219 nm rather than 208 nm). We note that 219 nm is resonant with a higher lying S_n excited state in BZA but that 208 nm is not. Therefore at 219 nm, a photoelectron spectrum from a *probe*−pump process (dotted line) is observed (i.e., the probe beam preceded the pump beam, hence

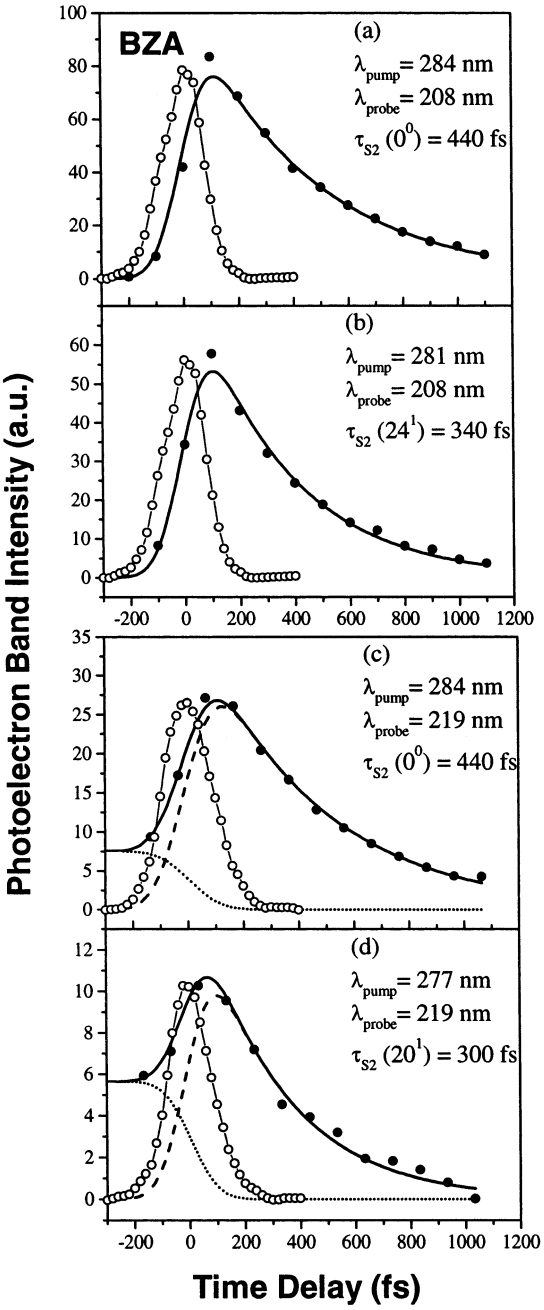

Figure 4. Time-dependent $S_2(\pi\pi^*)$ photoelectron band integral yields for BZA. The pump and probe laser wavelengths are indicated. Open circles indicate the cross-correlation functions measured at the same wavelengths: their fwhm range from 180 to 210 fs. The best fit (solid line) yields the time constants for the $S_2(\pi\pi^*)$ states. (a) Excitation to the $S_2(0^0)$ vibrationless origin. (b) Excitation to the $S_2(24^1)$ vibrational state, showing faster decay with increasing vibrational energy. (c) Excitation to the $S_2(0^0)$ vibrationless origin but with a longer (219 nm) probe laser wavelength. In this case both *pump−probe* (dashed, toward positive time) and *probe−pump* (dotted, toward negative time) signals are seen. The overall fits yields identical (±8 fs) time constants to the shorter (208 nm) probe wavelength seen in part a. This confirms the accuracy of our fitting procedure and demonstrates that the results are unaffected by ionization dynamics. (d) Excitation to the $S_2(20^1)$ vibrational state, showing faster decay with increasing vibrational energy.

signal toward negative time delays), requiring a deconvolution technique to extract the shortest time constants. From comparison of parts a and c of Figure 4, we see that the fits to the pump−probe process (positive delay times) yield the same decay constant (440 fs) within experimental error (±8 fs). This

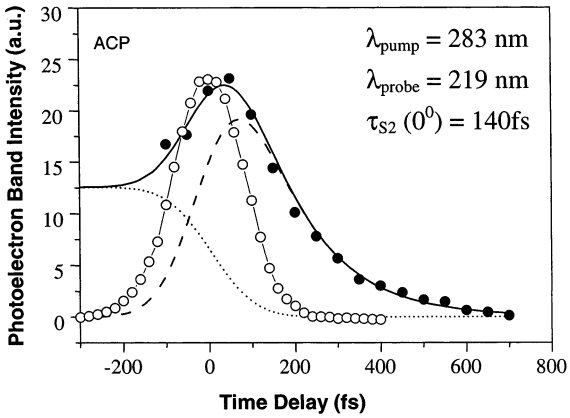

Figure 5. Time-dependent $S_2(\pi\pi^*)$ photoelectron band integral yields for excitation of ACP to the $S_2(0^0)$ vibrationless origin, showing the C═O group enhancement of the electronic relaxation rate as compared with BZA in Figure 4. The pump and probe laser wavelengths are indicated. Open circles indicate the cross-correlation functions measured at the same wavelengths. The best fit (solid line) yields the time constant for the $S_2(\pi\pi^*)$ state.

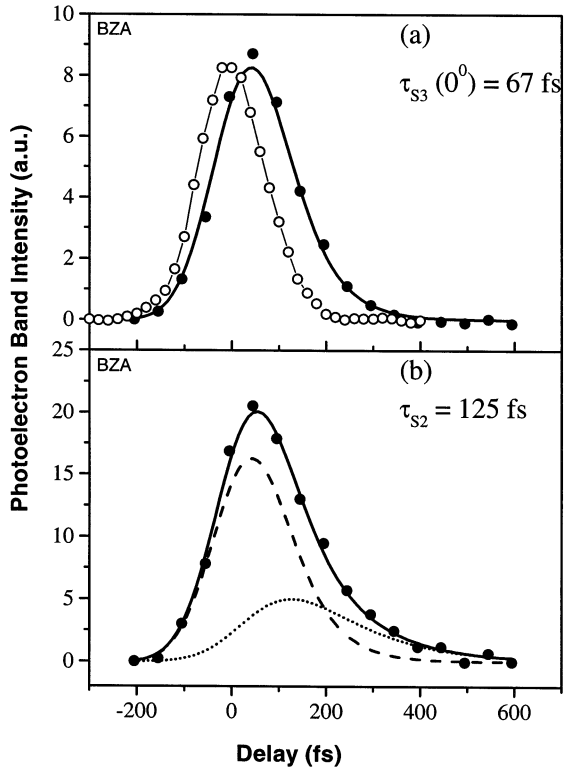

Figure 6. (a) Time-dependent $S_3(\pi\pi^*)$ 0^0 photoelectron band integral yields for BZA with $\lambda_{pump} = 242$ nm and $\lambda_{probe} = 219$ nm. The partial integration (solid line) over a nonoverlapped 0.70−1.35 eV higher energy range is assigned to S_3 ionization. Open circles represent the cross-correlation (CC) function at these wavelengths. (b) Time-dependent BZA integral photoelectron yield over a 0−0.35 eV range, under the same experimental conditions as in part a; the dotted line is obtained by subtraction of the contribution from state $S_3(\pi\pi^*)$ (dashed line) from the total integration. The dotted line, with fitted time constant of 125 fs, is assigned to the $S_2(\pi\pi^*)$ state.

demonstrates our ability to extract accurate time constants from multicomponent fits. Perhaps even more importantly, the fact that identical time constants are obtained for the 208 nm (Figure 4a) and 219 nm (Figure 4c) probe means that the ionization dynamics are very likely direct and not significantly contaminated by the autoionization of superexcited states.

To illustrate the effect of the substituent, the time-dependent photoelectron yield of acetophenone (ACP) excited to its

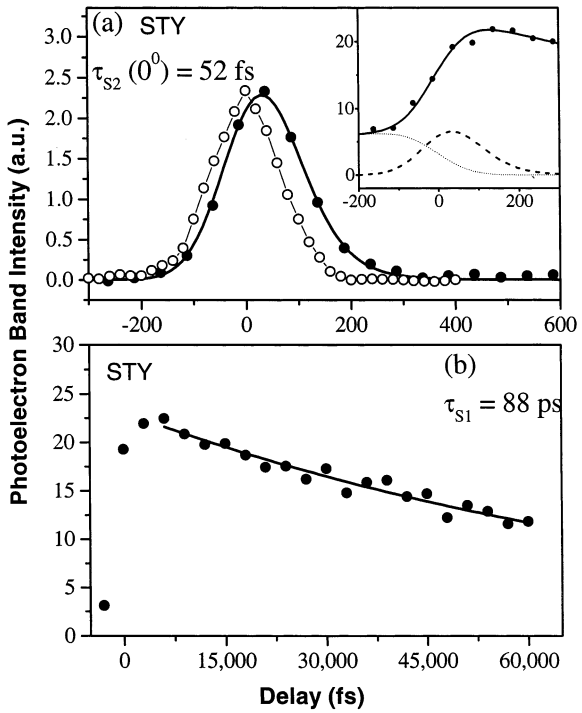

Figure 7. (a) Time-dependent $S_2(\pi\pi^*)$ 0^0 photoelectron band integral yields for STY with $\lambda_{pump} = 254.3$ nm and $\lambda_{probe} = 218.5$ nm, obtained via partial integration over the nonoverlapped 1.55−2.20 eV higher energy range. The corresponding time-resolved photoelectron spectrum is shown in Figure 3. [Inset: Integration over the total photoelectron yield (closed circles) at short time delays. The solid line is the best fit. The dotted line is the best fit to the $S_1(\pi\pi^*)$ component. The dotted line represents the *probe*−*pump* process, as discussed in Figure 4. The dashed line is the best fit to the $S_2(\pi\pi^*)$ channel, yielding the decay time constant of 52 fs]. Open circles represent the CC at these same wavelengths. (b) Time-dependent $S_1(\pi\pi^*)$ photoelectron band integral yields for STY under the same experimental conditions as in part a, obtained from a fit to the long delay part of the data (not shown in Figure 3).

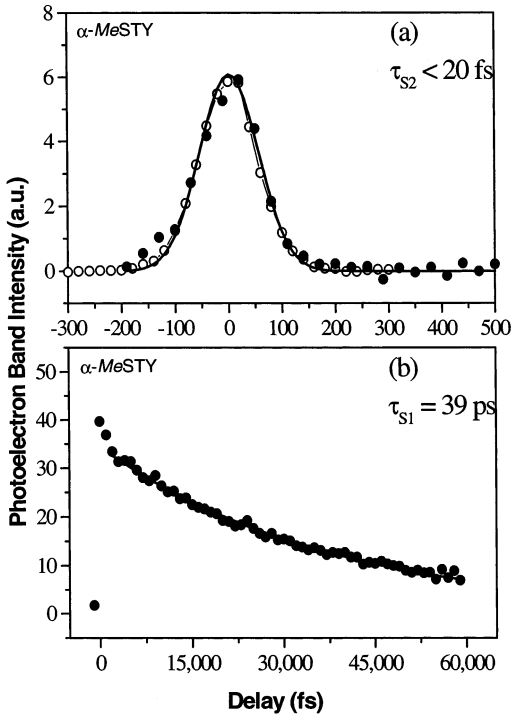

Figure 8. (a) Time-dependent $S_2(\pi\pi^*)$ photoelectron band integral yields for α-MeSTY with $\lambda_{pump} = 254$ nm and $\lambda_{probe} = 279$ nm, obtained via partial integration over the nonoverlapped 0.6−1.0 eV higher energy range. Symbols are as defined in Figure 7. Due to the Gaussian deconvolution procedure, we prefer not to accurately assign fitted time constants under 20 fs. (b) Time-dependent $S_1(\pi\pi^*)$ photoelectron band integral yields for α-MeSTY under the same experimental conditions as in part a, obtained from a fit to the long delay part of the data.

$S_2(\pi\pi^*)$ origin is shown in Figure 5. We see that this leads to the much faster electronic relaxation time constant of 140 ± 10 fs. The electronic relaxation of the second $\pi\pi^*$ state (S_3) of BZA is shown in Figure 6a. The subsequent electronic relaxation of the S_2 state formed by internal conversion of S_3 is shown in Figure 6b. Similarly, time-resolved S_n electronic population spectra for styrene (STY), α-methylstyrene (α-MeSTY), indene (IND), and phenylacetylene (ϕACT), each excited near their $S_2(\pi\pi^*)$ origins, are shown in Figures 7, 8, 9, and 10, respectively.

We note that the fitted time constant for α-MeSTY is 18 ± 3 fs, significantly smaller than for the other molecules. Although we assumed Gaussian cross-correlation functions in these fits, it is difficult to ensure that there are no systematic (i.e., non-Gaussian) errors in the fit at such short time scales. In view of this fact, we therefore prefer to state that the electronic lifetime of the S_2 state of α-MeSTY is <20 fs. The extracted time constants for these six compounds at the various excitation wavelengths shown in Figures 4−9 are summarized in Table 3. For comparison, the decay time constants of benzene obtained by Radloff et al.[12] are also given. The lifetimes of the second $\pi\pi^*$ state range in the present work from <20 to 67 fs. For the C═C and C≡C substituted benzenes, the first $\pi\pi^*$ state exhibits long lifetimes, ranging from 9.4 to 274 ps. This contrasts with the first $\pi\pi^*$ states of the C═O-substituted benzenes, which exhibit ultrashort lifetimes: 440 fs for BZA and 140 fs for ACP. The measured $S_2(\pi\pi^*)$ lifetimes of BZA indicate a monotonic decrease with increasing S_2 vibrational energy, and no evidence for mode-specific vibrational enhancement was observed.

V. Discussion

To compare our results using time-resolved photoelectron spectroscopy with previously published work, we plot in Figure 11 the electronic relaxation rates versus vibrational energy of the first $\pi\pi^*$ states of the derivatives studied here. The measured decay rates of the non-carbonyl derivatives are quite similar to those of benzene at the same vibrational energy,[12,72,73] with the exception being IND, which relaxes more slowly due to its rigid structure. By contrast, as seen in Figure 11, the carbonyl derivatives display a much more rapid decay rate. The C═O substituent withdraws electrons from the phenyl ring and introduces low-lying $n\pi^*$ states that have a great effect on the electronic relaxation pathways. Overall, these results demonstrate that the TRPES method is quite well suited to the study of electronic relaxation processes, producing facile, direct, and accurate measurements of decay rates that are in agreement with the currently accepted understanding of aromatic physics. The results are discussed in more detail below.

The electronic relaxation rates of $S_1(\pi\pi^*)$ benzene, shown in Figure 11, include at low vibrational energies both $S_1 \rightarrow S_0$ fluorescence and the more dominant S_1-T_1 ISC.[74−76] The S_1-S_0 IC process becomes important starting at 2300 cm^{-1} vibrational energy,[41,42,73] and the rate increases sharply until ∼4000 cm^{-1}, after which it increases more slowly up to ∼12 000 cm^{-1}. This dramatic variation of decay rate with vibrational energy is attributed to the transition in the coupling mechanism from tunneling to surface hopping.[77,78] Below the surface crossing

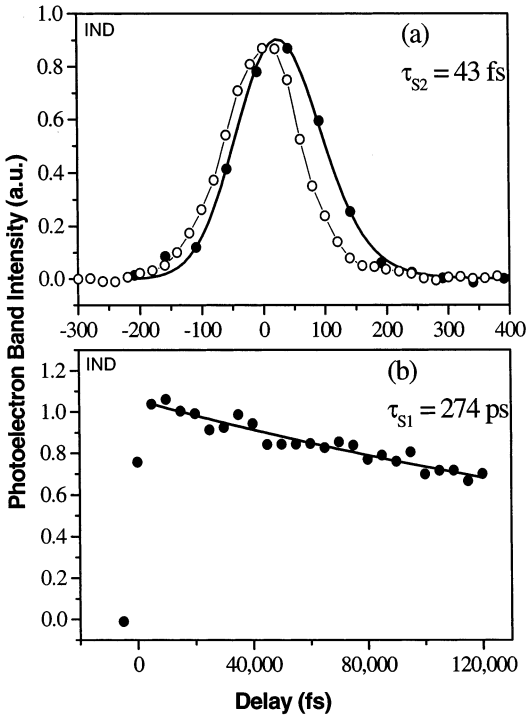

Figure 9. (a) Time-dependent $S_2(\pi\pi^*)$ photoelectron band integral yields for IND with $\lambda_{pump} = 254$ nm and $\lambda_{probe} = 219$ nm, obtained via partial integration over the nonoverlapped 1.95−2.55 eV higher energy range. (b) Time-dependent $S_1(\pi\pi^*)$ photoelectron band integral yields for IND under the same experimental conditions as in part a, obtained from a fit to the long delay part of the data. Symbols are the same as in Figure 7.

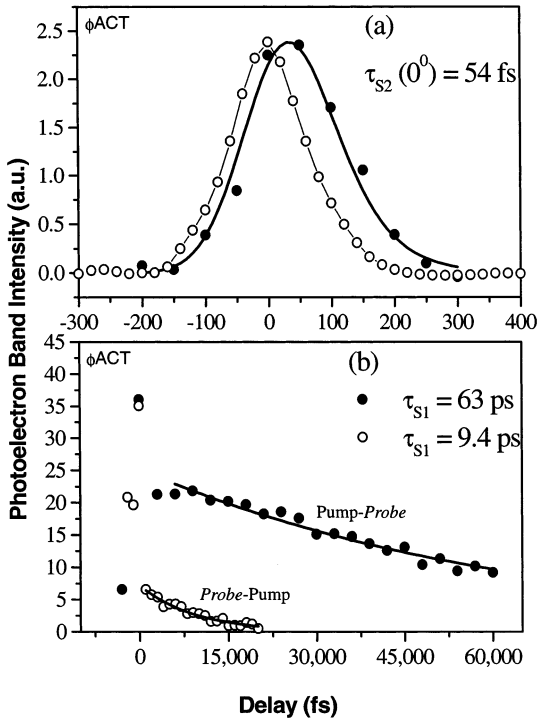

Figure 10. (a) Time-dependent $S_2(\pi\pi^*)$ 0^0 photoelectron band integral yields for ϕACT with $\lambda_{pump} = 238$ nm and $\lambda_{probe} = 219$ nm, obtained via partial integration over the nonoverlapped 1.35−2.10 eV higher energy range. (b) Time-dependent $S_1(\pi\pi^*)$ 0^0 photoelectron band integral yields. The solid circles denote the photoelectron yield from 0 to 2.10 eV for the *pump*−*probe* process with $\lambda_{pump} = 238$ nm and $\lambda_{probe} = 219$ nm. The open circles denote the photoelectron yield in the *probe*−*pump* process, i.e., with $\lambda_{pump} = 219$ nm and $\lambda_{probe} = 238$ nm, toward negative time delays but plotted here toward positive time. Symbols are the same as those defined in Figure 7.

point at ~4000 cm^{-1}, the system can tunnel through a barrier from the upper state to the lower electronic states. Above the crossing point, the system "hops" from one surface to another without abrupt changes in nuclear position or momentum. This change of coupling mechanism produces a marked change in the excess vibrational energy dependence of the electronic relaxation rate, with a smaller slope in the hopping region.

(A) Electronic Effects of the Substituent. Leopold et al.[58] measured jet-cooled absorption spectra to the second $\pi\pi^*$ state for STY, ϕACT, BZA, and ACP. Additionally, several $S_2(\pi\pi^*)$ vibronic bands of jet-cooled BZA[59] and ACP[60] were recorded by laser ionization and laser-induced fluorescence, respectively. The most prominent vibronic bands, arising mainly from motions in the substituent and substituent-sensitive ring modes, contrast with those in the first $\pi\pi^*$ transition, which primarily involves motions localized in the phenyl ring. According to vapor-phase absorption spectra of IND,[62] a diffuse system begins near 260.4 nm, and the position of the first observed broad band is assigned to the transition to the origin of the second $\pi\pi^*$ state. The diffuse vibronic bands in these systems suggest that the lifetimes of the second $\pi\pi^*$ state are rather short. This is consistent with our experimental data: the measured decay rates of the second $\pi\pi^*$ states are similar to that of benzene, except for α-MeSTY, which displays an even shorter lifetime. These findings suggest that a conical intersection between the first and the second $\pi\pi^*$ states is expected near the second $\pi\pi^*$ state minimum, as in benzene. The results of MC-SCF/4-31G calculations on benzene[69] show that the S_2-S_1 conical intersection is located above the minimum of $S_2(\pi\pi^*)$ by 9.1 kcal/mol. Likewise, theoretical results[85] based on a hybrid molecular mechanics−valence bond method indicate that the S_2-S_1 conical intersections for STY and IND are near the $S_2(\pi\pi^*)$ minimum, in agreement with our experimental data.

Benzene undergoes rapid $S_2(\pi\pi^*)$ decay at a rate of 1/50 fs^{-1} with a large energy gap $\Delta E(S_2-S_1) = 1.3$ eV, compared with that 0.57 eV in STY. Despite this large energy gap difference, both molecules have similar decay rates. (Recall that the $S_2(\pi\pi^*)$ lifetime of azulene[79,80] is ~2 ns with a large energy gap of $\Delta E(S_2-S_1) = 1.8$ eV). Clearly, the simple energy gap law fails to explain the electronic relaxation rates obtained in this work. For BZA, the $S_3(\pi\pi^*)$ 0^0 decay rate is 1/67 fs^{-1}, close to that of benzene at 1/50 fs^{-1}: this contrasts with the vastly different decay rates in their first $\pi\pi^*$ states.

BZA and ACP each have an additional $n\pi^*$ singlet state that is assigned to the first transition from a nonbonding orbital of oxygen to π^* of C═O chromophore. We investigated the energy dependence of electronic relaxation rates for three low-lying vibrational states plus one lying 6140 cm^{-1} above the $S_2(\pi\pi^*)$ origin in BZA. This highly excited vibrational state is expected to have poor Franck−Condon overlap for direct $S_0\rightarrow S_2(\pi\pi^*)$ electronic transitions, but can be prepared via $S_0\rightarrow S_3(\pi\pi^*)$ electronic transition, followed by rapid S_3-S_2 IC. In Figure 11 and Table 3, we can see that the $S_2(\pi\pi^*)$ decay rates of BZA and ACP increase monotonically with vibrational energy, showing no vibrational mode specificity. Comparing the $S_1(\pi\pi^*)$ decay of benzene with that of four non-carbonyl compounds at similar electronic energies, we found that the first $\pi\pi^*$ state of BZA has a decay rate 2.4×10^5 times greater than that of benzene at the origin and 400 times greater than that of benzene at 6000 cm^{-1} vibrational energy. BZA and ACP also show a $S_1(\pi\pi^*)$ decay rate 3.3×10^4 times greater than that of STY; the lifetime of which was estimated to be ~14.6 ns in 3-methylpentane solvent.[81]

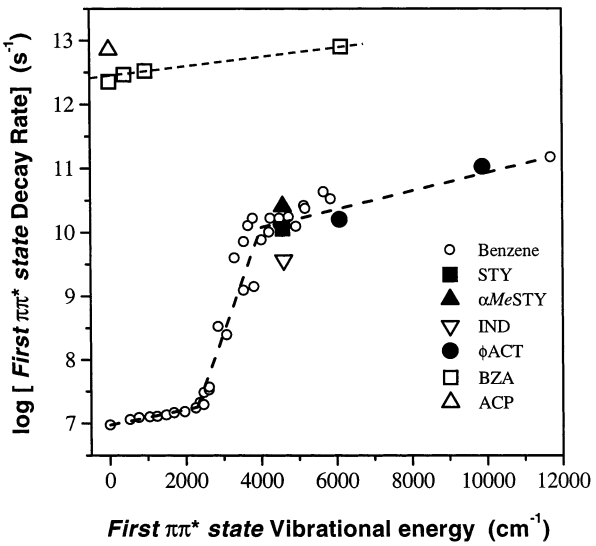

Figure 11. Excess vibrational energy dependence of the electronic relaxation rate of the first $\pi\pi^*$ state of benzene and its derivatives. Symbols ○, ■, ▲, ▼, ●, □, and △ denote benzene, STY, α-MeSTY, IND, ϕACT, BZA, and ACP, respectively. The log($1/\tau$) decay rates of benzene (○) are adopted from refs 12, 32, and 73. The lines are linear fits to these data over the energy ranges 0−2300, 2300−4000, and 4000−12 000 cm^{-1} in order to emphasize the marked change in decay rate vs vibrational energy (channel 3 decay). In this plot α-MeSTY is assumed to have the same vibrational energy as that in STY. These data suggest that the first $\pi\pi^*$ states of STY, α-MeSTY, IND, and ϕACT electronically relax essentially via benzene ring dynamics. By contrast, the first $\pi\pi^*$ states of BZA and ACP electronically relax *orders of magnitude* faster, indicating a completely different and extremely efficient mechanism. This is due to the presence of low-lying nπ^* states in BZA and ACP, absent in the other systems, which led to ultrafast intersystem crossing and the formation of triplet states.

It is instructive to compare the heteroatom effects in BZA and ACP with other heteroatom systems. The lifetime of high-lying vibrational levels of $S_1(n\pi^*)$ states of the azabenzenes pyridine, pyrazine, and pyrimidine near their $S_2(\pi\pi^*)$ origin were estimated to be 1.3, 17, and 35 ps, respectively. In direct $S_2(\pi\pi^*)$ excitation, it was assumed that the $S_2(\pi\pi^*)-S_1(n\pi^*)$ IC rate is much more rapid than the $S_1(n\pi^*)$ decay rate.[33] Theoretical calculations on pyrazine[43] indicate that the $S_1(n\pi^*)$ PES intersects the $S_2(\pi\pi^*)$ surface near the S_2 minimum and, via the $\nu_{10a}(B_{1g})$ vibrational mode, form a conical intersection.[82] Theoretical results[43] also indicate that the pyrazine $S_2(\pi\pi^*)$ surface exhibits a behavior similar to that of the benzene $S_1(\pi\pi^*)$ surface, the latter correlating with the ground state of the prefulvenic form and, therefore, there exists no isomerization barrier in the reaction path. Hence, there are two pathways for rapid electronic relaxation in the pyrazine $S_2(\pi\pi^*)$ state. Experimentally, the $S_2(\pi\pi^*)$ absorption bands of pyrazine are completely diffuse,[33] in contrast with those of $S_1(\pi\pi^*)$ of benzene. This is also in agreement with theoretical results.[43] Consequently, for BZA and ACP, each with a low-lying $S_1(n\pi^*)$ state, their rapid electronic relaxation rates are much greater than that of benzene because (i) the isomerization pathway to the prefulvenic form has no barrier, as in the case of pyrazine, or (ii) because electronic relaxation to $S_1(n\pi^*)$ followed by rapid ISC to triplet states becomes important. Since $T_1(n\pi^*) \rightarrow S_0$ phosphorescence of BZA was observed upon $S_2(\pi\pi^*)$ excitation,[83] it was suggested that a $S_2(\pi\pi^*)-T_1(n\pi^*)$ relaxation channel may exist prior to phosphorescence.

From photodissociation studies of BZA near the $S_2(\pi\pi^*)$ origin,[84] the decay rate of triplet BZA was found to be 1.2×10^6 s^{-1} via a pump−probe ionization technique; a mechanism was proposed involving rapid electronic relaxation followed by the dissociation of triplet states into $C_6H_6(T_1)$ and CO(X) products. Furthermore, the photon emission lifetime of ACP is 540 ns upon excitation to the $S_2(\pi\pi^*)$ origin and 130 ns when excited at $S_2(\pi\pi^*)12_0^1$. These lifetimes greatly exceed the directly measured values, indicating that the emitting states likely contain significant triplet character.[60] Unfortunately, in our TRPES experiments on BZA and ACP $S_2(\pi\pi^*)$ excitation, the formation of the $S_1(n\pi^*)$ and the low-lying triplet states was not directly detected because there was insufficient photon energy for 1+1 ionization detection and insufficient probe laser intensity for 1+2 ionization detection of these. The $S_2(\pi\pi^*)$ relaxation pathways to either S_0 directly or via $S_1(n\pi^*)$ followed by ISC to triplet states cannot be differentiated in our experimental data. Theoretical calculations on coupling among these low-lying singlet and triplet electronic states would help to elucidate this mechanism.

(B) Effects of Substituent Rigidity. IND is a prototype for investigating the effects of ϕ-C═C torsion on IC rates by comparing it with STY.[85] IND has a rigid five-membered ring structure that inhibits deformation to the prefulvene-like geometry, consistent with our observed $S_1(\pi\pi^*)$ decay rate of 274 ps for IND, as compared with 88 ps for STY (see Table 3). Interestingly, a similar type of behavior appears to exist in the benzene dimer and benzene(ammonia)$_n$ clusters.[44,45] The results of MC-SCF/4-31G calculations on benzene[69] show that the S_1-S_0 conical intersection resides 14.2 kcal/mol above the $S_2(\pi\pi^*)$ minimum and 5.1 kcal/mol above the adjacent S_2-S_1 conical intersection; in STY the S_1-S_0 intersection is around 5.9 kcal/mol above the S_2-S_1 conical intersection.[86] Other theoretical studies[85] using hybrid molecular mechanics−valence bond methods show two S_1-S_0 conical intersections in STY lying 8.4 and 10.2 kcal/mol above the $S_2(\pi\pi^*)$ minimum. By contrast, in IND four conical intersections were found to lie at 20−23.4 kcal/mol above the $S_2(\pi\pi^*)$ minimum. The S_1-S_0 conical intersections in IND lie at higher energies than those in benzene and STY because out-of-plane motion is inhibited by the rigid five-membered ring. All calculations on STY and IND were performed at energies near the S_2 region, but the qualitative results are analogous to those for benzene. The similarity of these benzene derivatives leads us to expect that near the S_1 minimum of STY and IND there exists at least one S_1-S_0 conical intersection similar to that in benzene. The barrier to the prefulvene-like diradical form for IND might be greater than that for benzene because the more rigid structure inhibits out-of-plane motion.

We investigated the effect of floppy modes and internal rotation on electronic relaxation rates through a comparison of (i) ACP with BZA and (ii) α-MeSTY with STY. A methyl group should have only a small effect on the electronic energy. Thus, the vibrational energy of the coupled $S_1(\pi\pi^*)$ state can be assumed to be roughly the same for methlyated and non-methylated derivatives at the same excitation wavelength. The electronic energy of the second $\pi\pi^*$ state of ACP is only 212−362 cm^{-1} above that of BZA. The measured lifetime of the $S_2(\pi\pi^*)$ 0^0 state of ACP is 140 fs, consistent with a ≤260 fs estimate based on a linewidth in a laser-induced fluorescence spectrum.[60] Interestingly, the decay rate in ACP is *3 times* as rapid as that in BZA. The small increase in internal energy of 212−362 cm^{-1} should not account for this significant increase in decay rate. Likewise, the methyl effect in α-MeSTY compared with STY shows a similar *3-fold* enhancement for

$S_2(\pi\pi^*)$ 0^0 electronic relaxation (and ~2-fold enhancement for $S_1(\pi\pi^*)$ relaxation).

We have recently completed a detailed comparison of electronic relaxation rates in the following simpler linear α,β-enones: acrolein (i.e., propenal), methyl vinyl ketone (i.e., α-methylpropenal), and crotonaldehyde (i.e., γ-methylpropenal).[87,88] Very dramatic effects on the electronic relaxation rates due to the location of the methyl group were observed: upon $S_2(\pi\pi^*)$ excitation, crotonaldehyde relaxed ~*5 times* more rapidly than either methyl vinyl ketone or acrolein. This methyl group enhancement observed in the α,β-enones appears qualitatively similar to our experimental findings here. One might expect in the Golden Rule sense that the methyl substituent increases the density of vibrational states and therefore a faster decay rate is obtained. However, as seen in Table 3, even when BZA has ~1000 cm^{-1} of excess vibrational energy, its electronic relaxation rate is still less than half of that of ACP at its vibrationaless origin. Furthermore, the identical number of degrees of freedom in methyl vinyl ketone and crotonaldehyde suggest that vibrational density of states is not the dominant effect. The methyl effect on the torsional conical intersections could be due to a change in diabatic vs adiabatic torsional dynamics at the conical intersection[87] (an inertial effect) and/or to a very subtle reordering of the conical intersections upon methylation[89] (an electronic effect). We speculate that this methyl group effect on C=C conical intersections seen in the α,β-enones is of a more general paradigm. If so, it is worthy of further investigation, as these simple substitutions could be used to provide an important new type of control over the electronic branching ratios that determine the efficiency of active MSE systems.

(C) Electronic Population Dynamics. As a final point, we consider the relative intensities of the photoelectron bands ϵ_n and ϵ_{n-1}. We observed electronic relaxation dynamics in the S_n and S_{n-1} states. The subsequent dynamics in lower lying states (S_{n-2} or T_k) were not *directly* detected, due to poor FC overlap with the cationic states. Their effects, however, were seen in the electronic relaxation dynamics of the S_{n-1} states. We consider the relative time-dependent electronic populations $P_n(t)$ and $P_{n-1}(t)$ of the S_n and S_{n-1} states, respectively, in a very simple consecutive reaction model:

$$S_n \xrightarrow{\tau_n} S_{n-1} \xrightarrow{\tau_{n-1}} S_{n-2}\ (\text{or } \Sigma T_k)$$

$$P_n(t) = P_n(0)\exp(-t/\tau_n)$$

$$P_{n-1}(t) = P_n(0)\tau_{n-1}/(\tau_n - \tau_{n-1})[\exp(-t/\tau_n) - \exp(-t/\tau_{n-1})] \quad (1)$$

$P_n(0)$ is the initial population of S_n created by femtosecond pump laser photoexcitation. *If* the ionization cross section of S_n is assumed to be approximately equal to that of S_{n-1}, their relative yields will be a function only of the measured decay time constants of the S_n and S_{n-1} states. For example, the amplitude of the $S_2(\pi\pi^*)$ component relative to that of $S_3(\pi\pi^*)$ can be evaluated from the ratios of their time constants. In BZA, we have observed that the measured amplitude of $S_2(\pi\pi^*)$ is only 25% of the value expected (based on the ratio of the time constants) relative to $S_3(\pi\pi^*)$. By contrast, for the hydrocarbon derivatives, the ratio of of the $S_1(\pi\pi^*)$ to $S_2(\pi\pi^*)$ amplitudes agrees with our predicted ratio. The $P_{n-1}(t)$ of STY, as shown in the inset of Figure 7a, is 3 times greater than $P_n(t)$, in contrast to BZA, for which the amplitude of the $P_{n-1}(t)$ component in Figure 6b is much less than that of $P_n(t)$. These experimental data indicate roughly that, for the hydrocarbon derivatives, $S_2(\pi\pi^*) \rightarrow S_1(\pi\pi^*)$ is a dominant decay pathway, but in BZA, by contrast, $S_3(\pi\pi^*) \rightarrow S_2(\pi\pi^*)$ is a minor channel. We note that this conclusion is valid only if the ionization cross-sections are roughly equal, and this is not obvious. However, supporting this picture, Hirata and Lim had previously suggested that in BZA, $S_1(n\pi^*)-S_0$ IC opens up and competes with $S_1(n\pi^*)-T_2(\pi\pi^*)/T_1(n\pi^*)$ ISC following $S_3(\pi\pi^*) \rightarrow S_1(n\pi^*)$ conversion (either directly or via $S_2(\pi\pi^*)$) because the phosphorescence quantum yield from the $T_1(n\pi^*)$ state decreases upon $S_3(\pi\pi^*)$ excitation.[83]

VI. Conclusion

We have investigated the applicability of femtosecond time-resolved photoelectron spectroscopy (TRPES) to the study of substituent effects in molecular electronic relaxation dynamics. We used a series of monosubstituted benzenes as model compounds, studying three basic types of electronic substituents: C=C (styrene), C=O (benzaldehyde), and C≡C (phenylacetylene). The effects of the rigidity and vibrational density of states of the substituent on the electronic relaxation dynamics were investigated via both methyl (α-methylstyrene, acetophenone) and alkyl ring (indene) substitution. The internal rotation degree of freedom of the methyl group was used to increase the density of states. The side alkyl ring structure in indene was used to add rigidity by enforcing planarity. From assignment of the energy-resolved photoelectron spectra, a fast decaying component was attributed to electronic relaxation of the second $\pi\pi^*$ state and a more slowly decaying component to the first $\pi\pi^*$ state populated by internal conversion from the higher lying state. Very fast electronic relaxation constants (<100 fs) for the second $\pi\pi^*$ states were observed for the electronic substituents C=C, C=O, and C≡C, more or less independent of the substituent and quite similar to that of benzene itself. Even a rigid ring substitution (indene) has no significant effect. This suggests a common decay mechanism involving the benzene ring, explained by relaxation to the first $\pi\pi^*$ via a conical intersection near the second $\pi\pi^*$ state planar minimum. The much slower vibrational energy-dependent electronic relaxation constants of the first $\pi\pi^*$ states for styrene and phenylacetylene are very similar to those of benzene in its first $\pi\pi^*$ state, at the same amount of vibrational energy. By contrast, the lifetime of the first $\pi\pi^*$ state of indene was greatly prolonged, and this was attributed to its rigid structure. The second $\pi\pi^*$ state of benzaldehyde has a very short lifetime, similar to that of the hydrocarbon compounds. However, the electronic relaxation of its first $\pi\pi^*$ state is orders of magnitude faster than that of any of the hydrocarbons. This is well-known and due to the oxygen heteroatom, which introduces a lower lying $n\pi^*$ state, greatly accelerating the electronic relaxation process.

A "floppy" methyl substitution (α-methylstyrene, acetophenone) might be expected to lead to even faster decay rates, through simple vibrational density of states arguments. The effect, however, is quite large (a factor of 3). Interestingly, we have observed similar methyl group enhancements in the smaller α,β-enones, where we have been able to rule out simple density of states arguments. We speculated that there could be a more interesting underlying photophysics and are currently pursuing this conjecture as it could have important consequences for the substitutional control of molecular electronic processes.

An important practical point is that variation of the ionization laser frequency had no effect on the photoelectron band shapes or lifetimes. This indicates that autoionization from superexcited

states played no important role in these measurements, thus allowing for a simple zeroth-order picture of the measurement based on Koopmans'-type ionization correlations. In general, our new results fit very well with the current understanding of aromatic photophysics, demonstrating that time-resolved photoelectron spectroscopy does provide for facile, accurate and, importantly, direct measurements of electronic relaxation dynamics in excited organic systems. We hope that, through judicious choices of model systems, the TRPES technique will help to develop a more detailed understanding of the important role of dynamical processes in molecular electronics.

Active molecular scale electronics (AMSE) is particularly based upon *molecular processes* that couple rearrangements such as isomerization or proton transfer to changes in optical or electrical properties. Despite the worldwide effort in organic-based AMSE, the important practical issues of *efficiency* and *stability* have received scant attention. These in turn are determined by the competition between ultrafast electronic processes in excited organic molecules. We believe that the effects of substituents on electronic relaxation dynamics will be an important variable in the rational design of functioning AMSE devices. The "simple" rules underlying these processes, however, are still being worked out. Nevertheless, we believe that important new developments in both theory and experiment could lead to a renaissance in the understanding of excited-state dynamics in polyatomic molecules.

Acknowledgment. This work was supported by the Canada−Taiwan NSC−NRC Collaborative Research Program. S.-H. L. thanks the Academia Sinica, Taiwan, for a postdoctoral fellowship. K.-C.T. and I-C.C. thank the NSC (Taiwan), for financial support. M.S. thanks the DFG (Germany), and T.S., J.G.U. and J.P.S. thank the NSERC (Canada) Visiting Fellowships Program for financial support.

References and Notes

(1) For example: Jortner, J.; Ratner, M. A. *Molecular Electronics* (IUPAC, Blackwell Oxford, 1997).

(2) For example: Stock, G.; Domcke, W. *Adv. Chem. Phys.* **1997**, *100*, 1 and references therein.

(3) Hayden, C. C.; Stolow, A. In *Adv. Series in Physical Chemistry Vol. 10: Photoionization and Photodetachment*; Ng, C. Y., Ed.; World Scientific: Singapore, 2000.

(4) Seel, M.; Domcke, W. *J. Chem. Phys.* **1991**, *95*, 7806.

(5) Cyr, D. R.; Hayden, C. C. *J. Chem. Phys.* **1996**, *104*, 771.

(6) Fischer, I.; Villeneuve, D. M.; Vrakking, M. J. J.; Stolow, A. *J. Chem. Phys.* **1995**, *102*, 5566.

(7) Fischer, I.; Vrakking, M. J. J.; Villeneuve, D. M.; Stolow, A. *Chem. Phys.* **1996**, *207*, 331.

(8) Engel, V. *Chem. Phys. Lett.* **1991**, *178*, 130; Meier, C.; Engel, V. *Chem. Phys. Lett* **1993**, *212*, 691; *J. Chem. Phys.* **1994**, *101*, 2673; *Phys. Rev. Lett.* **1994**, *73*, 3207.

(9) Baumert, T.; Thalweiser, R.; Gerber, G. *Chem. Phys. Lett.* **1993**, *209*, 29; Assion, A.; et al. *Phys. Rev. A* **1996**, *54*, R4605.

(10) Greenblatt, B. J.; Zanni , M. T.; Neumark, D. M. *Chem. Phys. Lett.* **1996**, *258*, 523.

(11) Smith, J. M.; Lakshminarayan, C.; Knee, J. L. *J. Chem. Phys.* **1990**, *93*, 4475; Zhang, X.; Smith, J. M.; Knee, J. L. *J. Chem. Phys.* **1994**, *100*, 2429; Lakshminarayan, C.; Knee, J. L. *J. Phys. Chem.* **1995**, *99*, 1768.

(12) Radloff, W.; Stert, V.; Freudenberg, Th.; Hertel, I. V.; Jouvet, C.; Dedonder-Lardeux, C.; Solgadi, D. *Chem. Phys. Lett.* **1997**, *281*, 20.

(13) Blanchet, V.; Stolow, A. In *Ultrafast Phenomena XI*; Elsaesser, T., Fujimoto, J. G., Wiersma, D. A., Zinth, W., Eds.; Springer: Berlin, 1998; p 456.

(14) Blanchet, V.; Zgierski, M. Z.; Seideman, T.; Stolow, A. *Nature* **1999**, *401*, 52.

(15) Schick, C. P.; Carpenter, S. D.; Weber, P. M. *J. Phys. Chem. A* **1999**, *103*, 10470.

(16) Sert, V.; Radloff, W.; Schultz, C. P.; Hertel, I. V. *Eur. Phys. J. D* **1999**, *5*, 97.

(17) Blanchet, V.; Zgierski, M. Z.; Stolow, A. *J. Chem. Phys.* **2001**, *114*, 1194.

(18) Schmitt, M.; Lochbrunner, S.; Shaffer, J. P.; Larsen, J. J.; Zgierski, M. Z.; Stolow, A. *J. Chem. Phys.* **2001**, *114*, 1206.

(19) Dobber, M. R.; Buma, W. J.; de Lange, C. A. *J. Phys. Chem.* **1995**, *99*, 1671.

(20) Blanchet, V.; Stolow, A. *J. Chem Phys.* **1998**, *108*, 4371.

(21) Kim, B.; Schick, C. P.; Weber, P. M. *J. Chem. Phys.* **1995**, *103*, 6903.

(22) Suzuki, T.; Wang, L.; Kohguchi, H. *J. Chem. Phys.* **1999**, *111*, 4859.

(23) Greenblatt, B. J.; Zanni, M. T.; Neumark, D. M. *Science* **1997**, *276*, 1675.

(24) Lochbrunner, S.; Schultz, T.; Schmitt, M.; Shaffer, J. P.; Zgierski, M. Z.; Stolow, A. *J. Chem. Phys.* **2001**, *114*, 2519.

(25) Reid, K. L. *Chem. Phys. Lett.* **1993**, *215*, 25; Reid, K. L.; Duxon, S. P.; Towrie, M. *Chem. Phys. Lett.* **1994**, *228*, 351;. Reid, K. L.; Field, T. A.; Towrie, M.; Matousek, P. *J. Chem. Phys.* **1999**, *111*, 1438.

(26) Seideman, T. *J. Chem. Phys.* **1997**, *107*, 7859; Althorpe, S. C.; Seideman, T. *J. Chem. Phys.* **1999**, *110*, 147.

(27) Arasaki, Y.; Takatsuka, K.; Wang, K.; McKoy, V. *Chem. Phys. Lett.* **1999**, *302*, 363.

(28) Davies, J. A.; LeClaire, J. E.; Continetti, R. E., Hayden, C. C. *J. Chem. Phys.* **1999**, *111*, 1.

(29) For example: Eland, J. H. D. *Photoelectron Spectroscopy;* Butterworths: London, 1984.

(30) Blanchet, V.; Lochbrunner, S.; Schmitt, M.; Shaffer, J. P.; Larsen, J. J.; Zgierski, M. Z.; Seideman, T.; Stolow, A. *Faraday Discuss.* **2000**, *115*, 33.

(31) Lim, E. C. In *Advances in Photochemistry*; Neckers, D. C., Ed.; Wiley: New York, 1997; Vol. 23, pp 165−211, and references therein.

(32) Stephenson, T. A.; Rice, S. A. *J. Chem. Phys.* **1984**, *81*, 1073.

(33) Yamazaki, I.; Murao, T.; Yamanaka, T.; Yoshihara, K. *Faraday Discuss. Chem. Soc.* **1983**, *75*, 395, and references therein.

(34) El-Sayed, M. A. *J. Chem. Phys.* **1962**, *36*, 573.

(35) El-Sayed, M. A. *J. Chem. Phys.* **1963**, *38*, 2832.

(36) El-Sayed, M. A. In *Excited States*; Lim, E. C., Ed.; Academic: New York, 1974; Vol. 1, pp 35−77, and references therein.

(37) Schubert, V.; Riedle, E.; Neusser, H. J. *J. Chem. Phys.* **1986**, *84*, 6182.

(38) Riedle, E.; Weber, Th.; Schuett, U.; Neusser, H. J.; Schlag, E. W. *J. Chem. Phys.* **1990**, *93*, 967.

(39) Otis, C. E.; Knee, J. L.; Johnson, P. M. *J. Chem. Phys.* **1983**, *78*, 2091.

(40) Knee, J. L.; Otis, C. E.; Johnson, P. M. *J. Chem. Phys.* **1984**, *81*, 4455.

(41) Callomon, J. H.; Perkins, J. E.; Lopez-Delgado, R. *Chem. Phys. Lett.* **1972**, *13*, 125.

(42) Nakashima, N.; Yoshihara, K. *J. Chem. Phys.* **1982**, *77*, 6040.

(43) Sobolewski, A. L.; Woywod, C.; Domcke, W. *J. Chem. Phys.* **1993**, *98*, 5627.

(44) Radloff, W.; Freudenberg, Th.; Ritze, H.-H.; Stert, V.; Noack, F.; Hertel, I. V. *Chem. Phys. Lett.* **1996**, *261*, 301.

(45) Radloff, W.; Freudenberg, Th.; Ritze, H.-H.; Stert, V.; Weyers, K.; Noack, F. *Chem. Phys. Lett.* **1995**, *245*, 400.

(46) Schultz, T.; Shaffer, J. P.; Schmitt, M.; Quenneville, J.; Martinez, T. J.; Zgierski, M. Z.; Stolow, A. Manuscript in preparation.

(47) Fuss, W.; Haas, Y.; Zilberg, S. *Chem. Phys.* **2000**, *259*, 273, and references therein.

(48) Leopold, D. G.; Pendley, R. D.; Roebber, J. L.; Hemley, R. J.; Vaida, V. J. *Chem. Phys.* **1984**, *81*, 4218.

(49) Hayden, C. C.; Chandler, D. W. *J. Phys. Chem.* **1995**, *99*, 7897.

(50) Petek, H.; Bell, A. J.; Christensen, R. L.; Yoshihara, K. *J. Chem. Phys.* **1992**, *96*, 2412.

(51) Kohler, B. E.; Terpougov, V. *J. Chem. Phys.* **1996**, *104*, 9297.

(52) Heimbrook, L. A.; Kohler, B. E.; Levy, I. J. *J. Chem. Phys.* **1984**, *81*, 1592.

(53) Petek, H.; Bell, A. J.; Yoshihara, K. *J. Chem. Phys.* **1991**, *95*, 4739.

(54) Bouwman, W. G.; Jones, A. C.; Phillips, D. *J. Phys. Chem.* **1990**, *94*, 7429.

(55) Andersson, P. O.; Bachilo, S. M.; Chen, R.-L.; Gillbro, T. *J. Phys. Chem.* **1995**, *99*, 16199.

(56) Bachilo, S. M.; Spangler, C. W.; Gillbro, T. *Chem. Phys. Lett.* **1998**, *283*, 235.

(57) Frank, H. A.; Farhoosh, R.; Gebhard, R.; Lugtenburg, J.; Gosztola, D.; Wasielewski, M. R. *Chem. Phys. Lett.* **1993**, *207*, 88.

(58) Leopold, D. G.; Hemley, R. J.; Vaida, V.; Roebber, J. L. *J. Chem. Phys.* **1981**, *75*, 4758.

(59) Silva, C. R.; Reilly, J. P. *J. Phys. Chem.* **1996**, *100*, 17111.

(60) Warren, J. A.; Bernstein, E. R. *J. Chem. Phys.* **1986**, *85*, 2365.

(61) Ribblett, J. W.; Borst, D. R.; Pratt, D. W. *J. Chem. Phys.* **1999**, *111*, 8454.

(62) Byrne, J. P.; Ross, I. G. *Aust. J. Chem.* **1971**, *24*, 1107.

(63) Dyke, J. M.; Ozeki, H.; Takahashi, M.; Cockett, M. C. R.; Kimura, K. *J. Chem. Phys.* **1992**, *97*, 8926.
(64) Chizhov, Y. V.; Timoshenko, M. M.; Kleimenov, V. I.; Borisov, Y. A.; Zolnikova, G. P.; Kravtsov, D. N.; Kritskaya, I. I. *J. Struct. Chem.* **1986**, *27*, 401.
(65) Kendler, S.; Ziberg, S.; Haas, Y. *Chem. Phys. Lett.* **1995**, *242*, 139.
(66) Klasinc, L.; Kovac, B.; Gusten, H. *Pure Appl. Chem.* **1983**, *55*, 289.
(67) Distefano, G.; Granozzi, G.; Bertoncello, R.; Olivato, P. R.; Guerrero, S. A. *J. Chem. Soc., Perkin Trans.* **1987**, *2*, 1459 .
(68) Salem, L. *The Molecular Orbital Theory of Conjugated Systems;* Benjamin: Reading, MA, 1966.
(69) Palmer, I. J.; Ragazos, I. N.; Bernardi, F.; Olivucci, M.; Robb, M. A. *J. Am. Chem. Soc.* **1993**, *115*, 673.
(70) Lochbrunner, S.; Larsen, J. J.; Shaffer, J. P.; Schmitt, M.; Schultz, T.; Underwood, J. G.; Stolow, A. *J. Electron Spectrosc. Relat. Phenom.* **2000**, *112*, 183.
(71) Zavriyev, A.; Fischer, I.; Villeneuve, D. M.; Stolow, A. *Chem. Phys. Lett.* **1995**, *234*, 281.
(72) O'Connor, D. V. *Faraday Discuss. Chem. Soc.* **1983**, *75*, 415.
(73) Sumitami, M.; O'Connor, D. V.; Takagi, Y.; Nakashima, N.; Kamogawa, K.; Udagawa, Y.; Yoshihara, K. *Chem. Phys.* **1985**, *93*, 359.
(74) Sekreta, E.; Reilly, J. P. *Chem. Phys. Lett.* **1988**, *149*, 482.
(75) Duncan, M. A.; Dietz, T. G.; Liverman, M. G.; Smalley, R. E. *J. Phys. Chem.* **1981**, *85*, 7.
(76) Otis, C. E.; Knee, J. L.; Johnson, P. M. *J. Chem. Phys.* **1983**, *78*, 2091.
(77) Kato, S. *J. Chem. Phys.* **1988**, *88*, 3045.
(78) Sobolewski, A. L. *J. Chem. Phys.* **1990**, *93*, 6433.
(79) Demmer, D. R.; Hager, J. W.; Leach, G. W.; Wallace, S. C. *Chem. Phys. Lett.* **1987**, *136*, 329.
(80) Diau, E. W.-G.; Feyter, S. D.; Zewail, A. H. *J. Chem. Phys.* **1999**, *110*, 9785.
(81) Condirston, D. A.; Laposa, J. D. *Chem. Phys. Lett.* **1979**, *63*, 313.
(82) Seidner, L.; Stock, G.; Sobolewski, A. L.; Domcke, W. *J. Chem. Phys*. **96**, 5298 1992.
(83) Hirata, Y.; Lim, E. C. *J. Chem. Phys.* **1980**, *72*, 5505.
(84) Silva, C. R.; Reilly, J. P. *J. Phys. Chem. A* **1997**, *101*, 7934.
(85) Bearpark, M. J.; Bernardi, F.; Olivucci, M.; Robb, M. A. *J. Phys. Chem. A* **1997**, *101*, 8395.
(86) Bearpark, M. J.; Olivucci, M.; Wilsey, S.; Bernardi, F.; Robb, M. A. *J. Am. Chem. Soc.* **1995**, *117*, 6944.
(87) Shaffer, J. P.; Schultz, T.; Schmitt, M.; Underwood, J. G.; Stolow, A. Untangling $\pi-\pi^*/n-\pi^*$ orbital interactions via time-resolved photoelectron spectroscopy. In *Springer Series in Chemical Physics*, *Vol. 64*, *Ultrafast Phenomena XII*; Elsaesser, T., Mukamel, S., Murnane, M., Scherer, N., Eds.; Springer-Verlag: Berlin, 2000.
(88) Shaffer, J. P.; Schmitt, M.; Schultz, T.; Zgierski, M. Z.; Chen, I−C. Olivucci, M.; Stolow, A. In preparation.
(89) Olivucci, M. Private communication.